Tokamak Rotation and Halo Current caused by Disruptions

H. Strauss, *HRS Fusion*

L. Sugiyama, *MIT*

R. Paccagnella, *Instituto Gas Ionizzati del C.N.R.*

J. Breslau, *PPPL*

S. Jardin, *PPPL*

Outline

- AVDE disruptions
  - resistive wall and sideways wall force
  - disruption time scales: VDE, thermal quench, current quench
  - VDE equilibrium and stability
  - mitigation: scalings of sideways force
- toroidal rotation in disruptions and ELMs
  - conservation of toroidal angular momentum
  - disruption simulations and theory
  - ELM simulations
  - intrinsic toroidal rotation
- halo current in disruptions
- velocity boundary conditions

H. Strauss, R. Paccagnella, J. Breslau, L. Sugiyama, S. Jardin, Sideways force produced during tokamak disruptions, Nuclear Fusion **53**, 073018 (2013).

AVDE disruptions

M3D and Resistive Walls

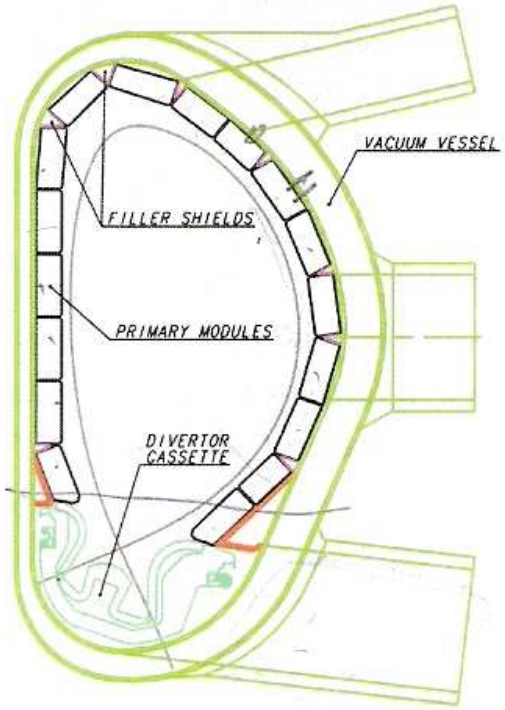

FIG. 1 Vacuum vessel and blanket module poloidal segmentation

Outside the outer wall the magnetic field is solved with GRIN, using Green's functions. Presently developing GRIN to have multiple walls.

- The plasma and blanket are bounded by thin resistive walls of thickness δ_{wall}, resistivity η_{wall} (different for each wall, and η_{wall} can be spatially varying.)
- Normal component of magnetic field B_n is continuous at walls.
- The normal magnetic field on the walls is time advanced with

$$\frac{\partial B_n}{\partial t} = -\hat{\mathbf{n}} \cdot \nabla \times (\eta_{wall} \mathbf{J}_{wall})$$

$$\tau_{wall} = \frac{b\delta_{wall}}{\eta_{wall}}$$

where b is a wall radius

- In the following, only one resistive wall is assumed, the first wall.

Wall Force

The current in the walls is given by the jump in the components of B tangential to the wall,

$$\mathbf{J}_w = \nabla \times \mathbf{B} \approx \frac{\hat{\mathbf{n}}}{\delta} \times \left[\mathbf{B}^{(+)} - \mathbf{B}^{(-)}\right].$$

where $^{(+)}$ is the outside and $^{(-)}$ is the inside of each wall.

The wall force is given by

$$\mathbf{F} = \delta \int d\phi \int dl R(\mathbf{J}_w \times \mathbf{B}_w). \tag{1}$$

Of particular importance is the horizontal force, $F_x = \hat{\mathbf{x}} \cdot \hat{\mathbf{F}}$ where $\hat{\mathbf{x}} = \hat{\mathbf{R}} \cos\phi - \hat{\phi} \sin\phi$. To get a nonzero F_x, there must be an $(m, n) = (1, 1)$ or $\exp(i\theta - i\phi)$ perturbation of the wall current, from $(\mathbf{J}_w \times \mathbf{B}_w \cdot \hat{\mathbf{n}})(\hat{\mathbf{n}} \cdot \hat{\mathbf{R}})(\hat{\mathbf{R}} \cdot \hat{\mathbf{x}}) \sim \cos(\theta)\cos(\phi)$.

In the simulations, F is normalized in units of $F_{dim} = 2\pi R_0 L_w B_0^2/\mu_0$, where $L_w = \int dl$ is the wall circumference.

AVDE disruption time scales

There are 3 time scales in AVDE (asymmetric vertical displacement event) disruptions

- τ_{wall} – resistive wall penetration time, VDE growth time. The VDE scrapes off magnetic flux, causing q at the last closed flux surface to drop to $q \approx 2$, causing the plasma to become ideal MHD unstable.

- γ^{-1} – growth time of $n = 1$ modes, predominantly $(2,1), (1,1)$. The modes cause the magnetic field to become stochastic, producing the thermal quench (TQ). Hence $\tau_{TQ} \approx \gamma^{-1} \approx 10^2 \tau_A$.

- τ_{halo} – the halo resistive (L/R) time. The TQ cools the plasma to the halo temperature, and the plasma resistively decays in time τ_{halo}, or the current is carried into the wall by the VDE, causing the current quench (CQ). $\tau_{CQ} = \min(\tau_{halo}, \tau_{wall})$

The plasma S is almost irrelevant, as long as it is large enough so that resistive mode growth rates are sufficiently slow.

VDE equilibrium

An initially VDE unstable ITER equilibrium, FEAT15MA, was evolved in 2D with M3D until $q \approx 2$ at the last closed flux surface.

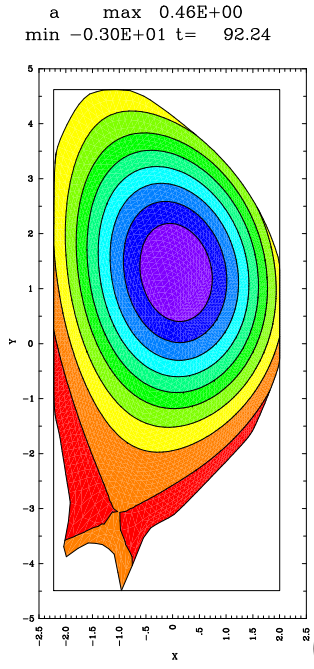

(a)

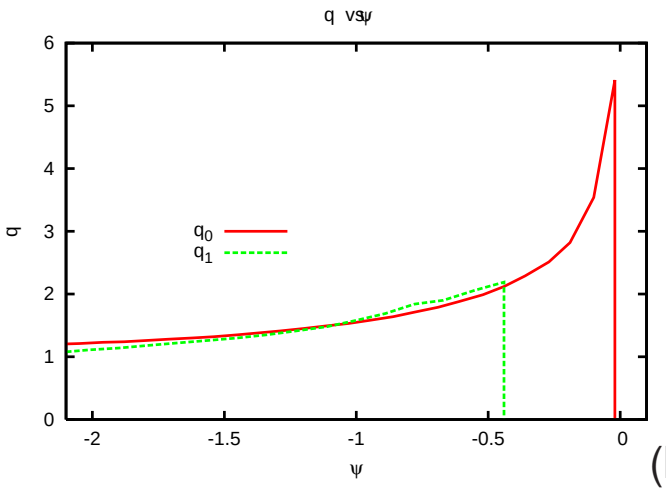

(b)

(a) The poloidal magnetic flux ψ is shown during a VDE.

(b) q profiles corresponding the initial state and (a). The vertical lines are drawn at the last closed flux surface.

Stability

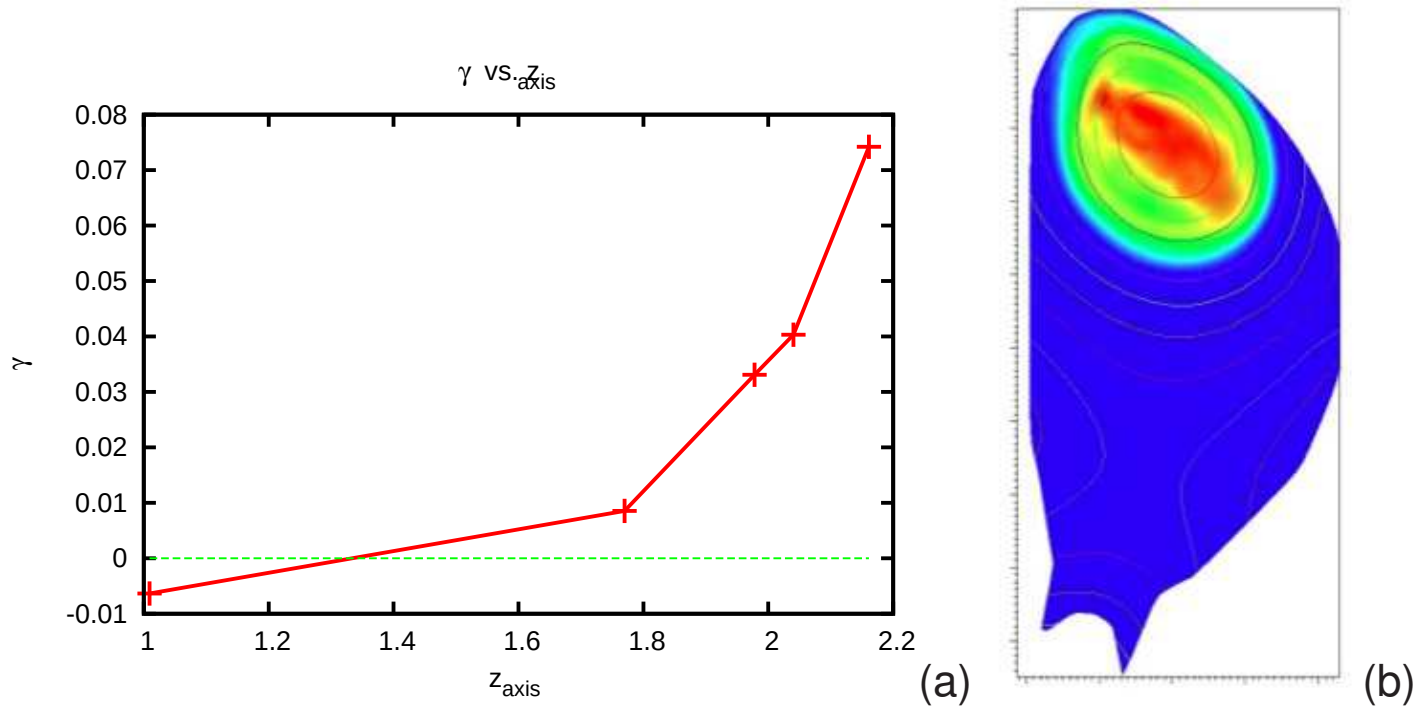

(a) The plasma is unstable to $n = 1$ modes. As the VDE displacement increases, q drops and the predominantly $(m, n) = (2, 1)$ mode growth rate increases. (b) Perturbed pressure in a nonlinear evolution. The mode structure is predominantly $(m, n) = (2, 1)$.

$F_x(\xi_{VDE})$

VDEs were evolved to different displacements, and plasma profiles changed to model MGI mitigation: toroidal current and pressure were set to zero outside $q = 2$ surface, but toroidal total current and pressure kept constant.

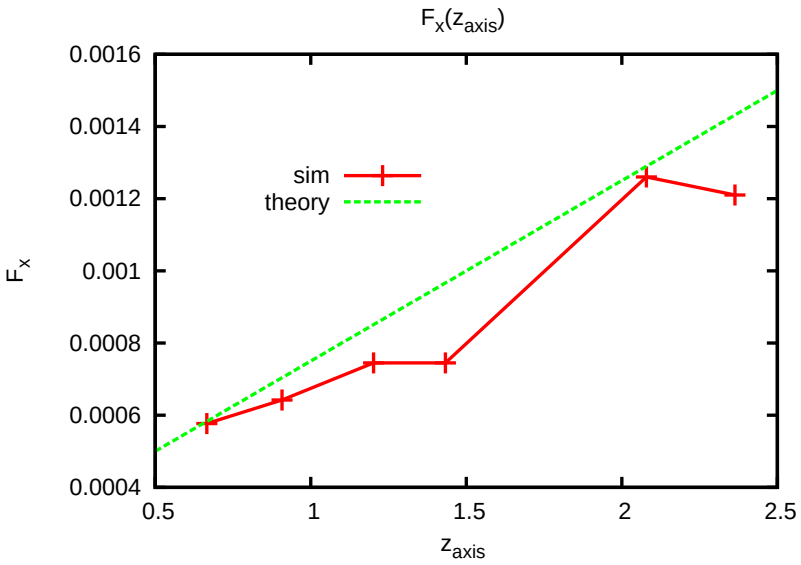

Force F_x as a function of VDE displacement ξ_{VDE}. The points on the solid line are from simulations. This shows $F_x \approx c_1\xi_{VDE} + c_2$. Mitigation of F_x is greatest when $\xi_{VDE} = 0$.

Sideways force depends on plasma displacement

$$\xi = \sum_{mn} \xi_{mn}(t) f_{mn}(r) \exp(im\theta - in\phi)$$

F_x produced by $\exp(i\theta - i\phi)$ displacement, from ξ_{11} and $\xi_{10}\xi_{21}$, where $\xi_{VDE} = \xi_{10}$.

$$F_x = c_{21}\frac{\xi_{VDE}}{b}\frac{\xi_{21}}{a} + c_{11}\frac{\xi_{11}}{a} \qquad (2)$$

[Strauss *et al.* 2013], where a = plasma radius, b = wall radius (circular cross section model), $q_0 = q$ plasma

$$c_{m1} = \left(\frac{a}{b}\right)^m \left(\frac{a}{q_0 R}\right)^2 \frac{\gamma_{m1}\tau_{wall}(1 - q_0)}{2m + (\gamma_{m1}\tau_{wall})[1 - (a/b)^{2m}]}$$

For $\gamma\tau_{wall} \gg 1$, $c_{11}, c_{21} \to$ constant.

$F_x(\gamma\tau_{wall})$ scaling

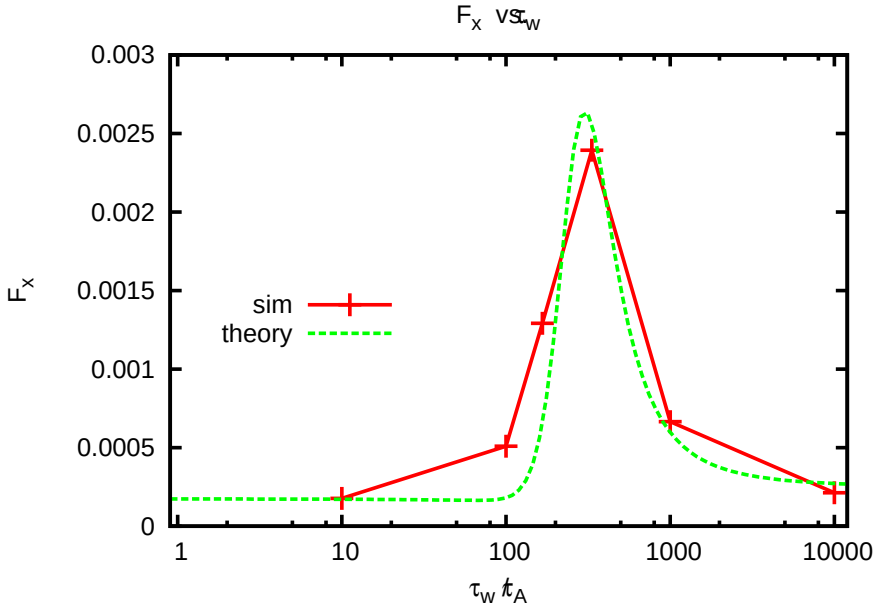

Force F_x as a function of τ_{wall}/τ_A.

Here the plasma is evolved from small VDE and $n = 1$ initial perturbations. The asymmetric wall force F_x is maximum when $\gamma\tau_{wall} \sim 1$.

Note that $\gamma \approx 0.01\tau_A^{-1}$.

Model the mode and VDE amplitudes assuming exponential growth and decay. The α terms are initial amplitudes at $t = 0$.

$$\xi_{21}/a = \mathrm{sech}(\gamma t - \alpha_{21}), \qquad \xi_{VDE}/b = \mathrm{sech}(t/\tau_w - \alpha_{VDE})$$

From (2) $F_x(t)$ is maximum when $\partial(\xi_{21}\xi_{VDE})/\partial t = 0$.

$$F_x \propto c_{21}\xi_{VDE}^{max}\xi_{21}^{max}\mathrm{sech}^2\left((\gamma\tau_w\alpha_{VDE} - \alpha_{21})/(1+\gamma\tau_w)\right) + bc_{11}\xi_{11}^{max}$$

Peak value of $F_x(\gamma\tau_w)$ occurs for $\gamma\tau_w = \alpha_{21}/\alpha_{VDE} \sim 1$, which depends on initial conditions. For $\gamma\tau_{wall} \gg 1$, there is a mitigating effect: $F_x^{min}/F_x^{max} \approx 0.1 \sim \xi_{11}/\xi_{21}$. In dimensional units $F_x^{max} \approx 60$ MN, the maximum tolerable by ITER.

DOE milestone: Time history of disruption

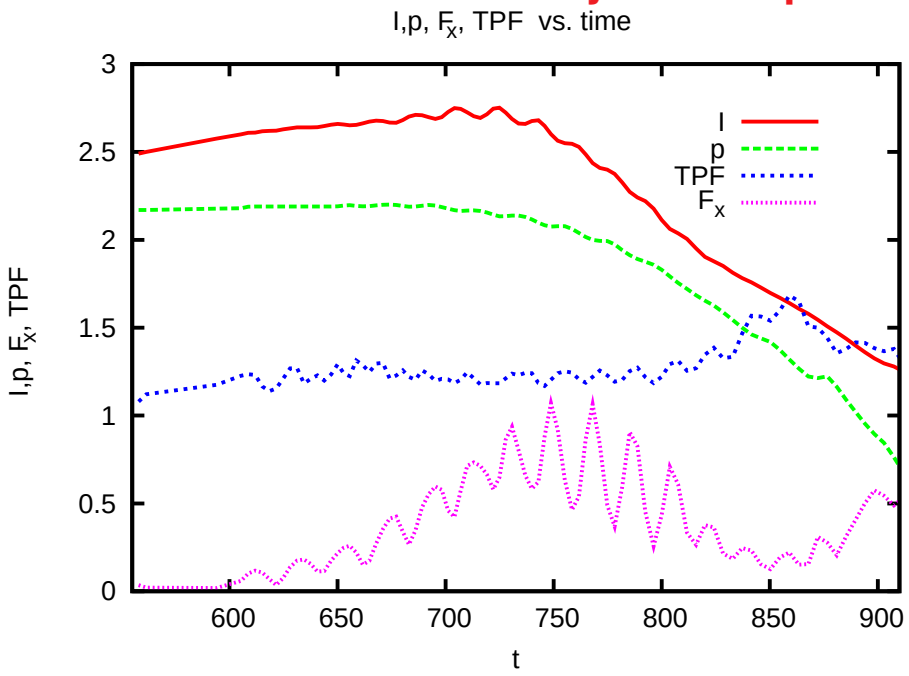

Time history of a DOE milestone (in progress) disruption simulation. Parameters: $S = 10^6, \tau_{wall} = 10^4 \tau_A, \tau_{halo} = 10^3 \tau_A$. Shown are normalized total current I, normalized total pressure p , and TPF. Also shown is F_x, the dimensionless sideways wall force multiplied by 10^4. $F_x \approx 3\%$ of the maximum F_x that can be tolerated by ITER. The value $\gamma\tau_{wall}$ is the rightmost point on the previous graph of $F_x(\gamma\tau_A)$. The oscillations of F_x are caused by toroidal rotation.

Model of external inductance (current controller) can give more time more separation of TQ and CQ.

Rotation in disruptions and ELMs

It was observed that disruptions were accompanied by toroidal rotation [Gerhardt 2012,Granetz 1996, Gerasimov 2010].

There is a concern that this rotation may occur during ITER disruptions, causing a resonance between rotating toroidal perturbations and the resonant frequencies of the vacuum vessel.

In an MHD model, disruptions (loss of equilibrium) can produce rotation.

Both toroidal and poloidal rotation are produced.

Toroidal rotation is sheared, peak value can be $10\times$ larger than average value. (MHD zonal flow).

MHD activity may produce intrinsic toroidal rotation [Rice 2007].

Conservation of toroidal angular momentum

$$\frac{\partial}{\partial t} L_\phi = \oint (R B_\phi B_n - \rho R v_\phi v_n) R dl d\phi \tag{3}$$

where the total toroidal angular momentum is

$$L_\phi = \int \rho R^2 v_\phi dR dZ d\phi \tag{4}$$

and the integral in (3) is over the boundary. Using the M3D magnetic field representation,

$$\mathbf{B} = \nabla\psi \times \nabla\phi + \frac{1}{R}\nabla_\perp F + G\nabla\phi \tag{5}$$

in (3) yields

$$\frac{\partial}{\partial t} L_\phi = \oint G \frac{\partial \psi}{\partial l} dl d\phi \tag{6}$$

where $\partial F/\partial n = 0$ at the boundary. We have assumed that $v_\phi = 0$ at the boundary, but not $v_n = 0$ at the boundary, although we have done so in simulations with M3D.

If $G = G(\psi)$, then toroidal angular momentum L_ϕ is conserved. This is the case in an equilibrium satisfying the Grad - Shafranov equation. If the plasma is not in equilibrium, such as during a disruption or ELM, then net flow can be generated.

VDE - kink disruption

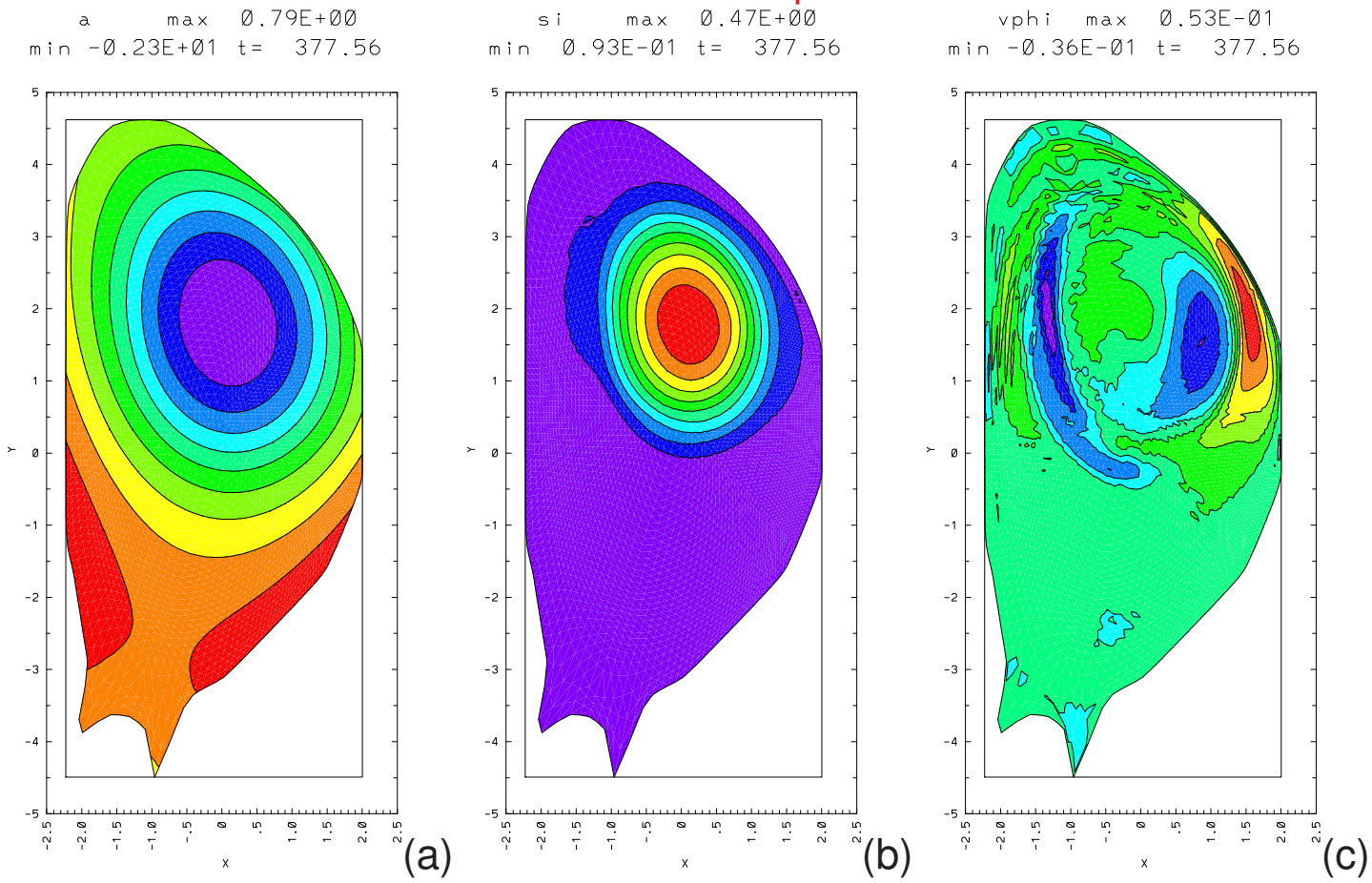

(a) The poloidal magnetic flux ψ during a disruption at toroidal angle $\phi = 0$, time $t = 377\tau_A$. Parameters: $S = 10^6, \tau_w = 10^3\tau_A, \tau_{halo} = 10^3\tau_A$. (b) Toroidal magnetic flux G at the same toroidal angle and the same time. The contours of G and ψ are different, indicating that toroidal angular momentum can be generated. (c) Toroidal velocity v_ϕ at the same toroidal angle and time. The flow is sheared; it is zero on axis and small near the wall.

VDE - kink disruption

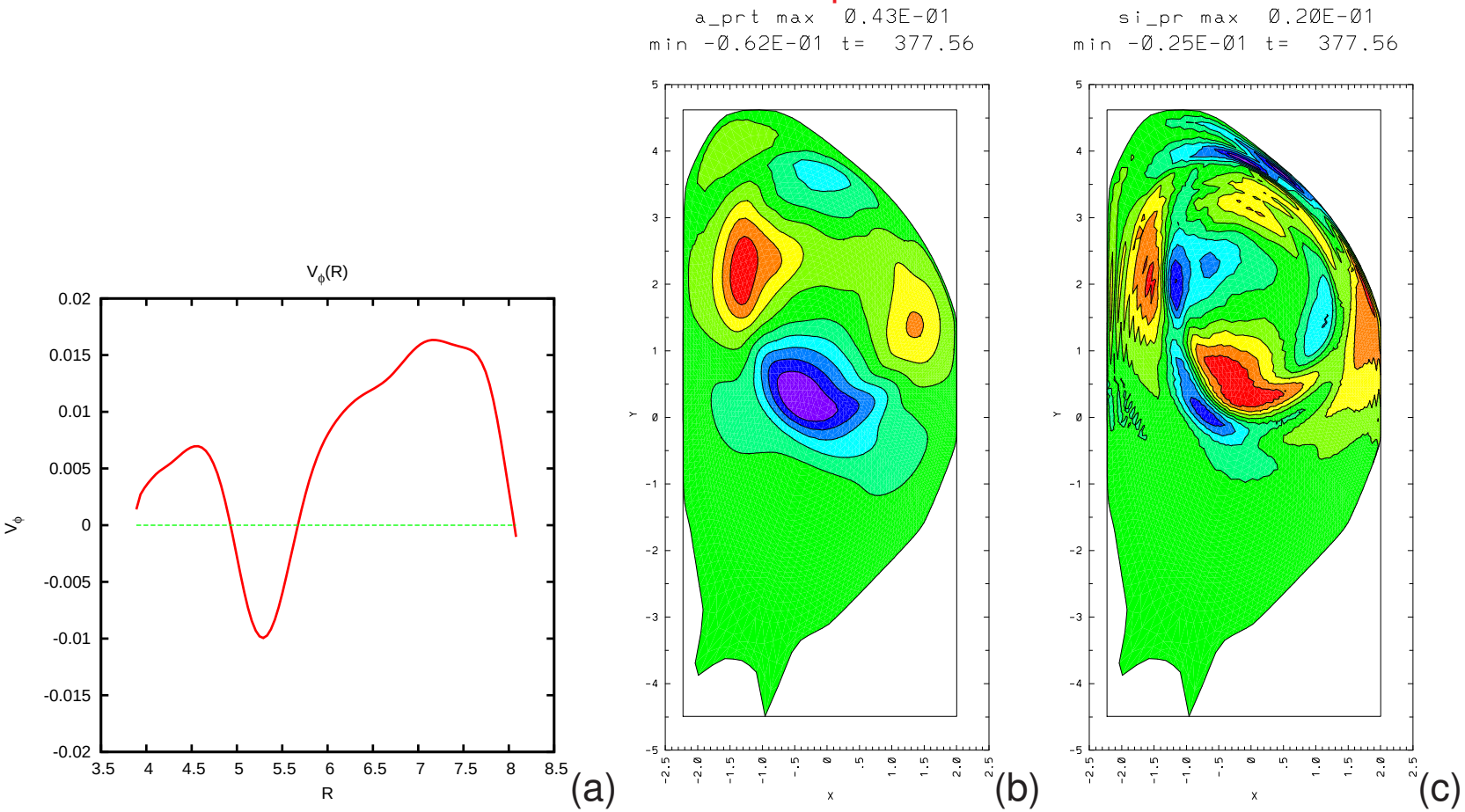

(a) slice plot of $v_\phi(R, 0, 0)$ at time $t = 377\tau_A$ showing sheared structure. (b) Toroidally varying part of ψ at the same time. (c) Perturbed toroidal magnetic flux G at the same toroidal angle and the same time. The contours of G and ψ are different, indicating that toroidal angular momentum can be generated.

Time history of disruption

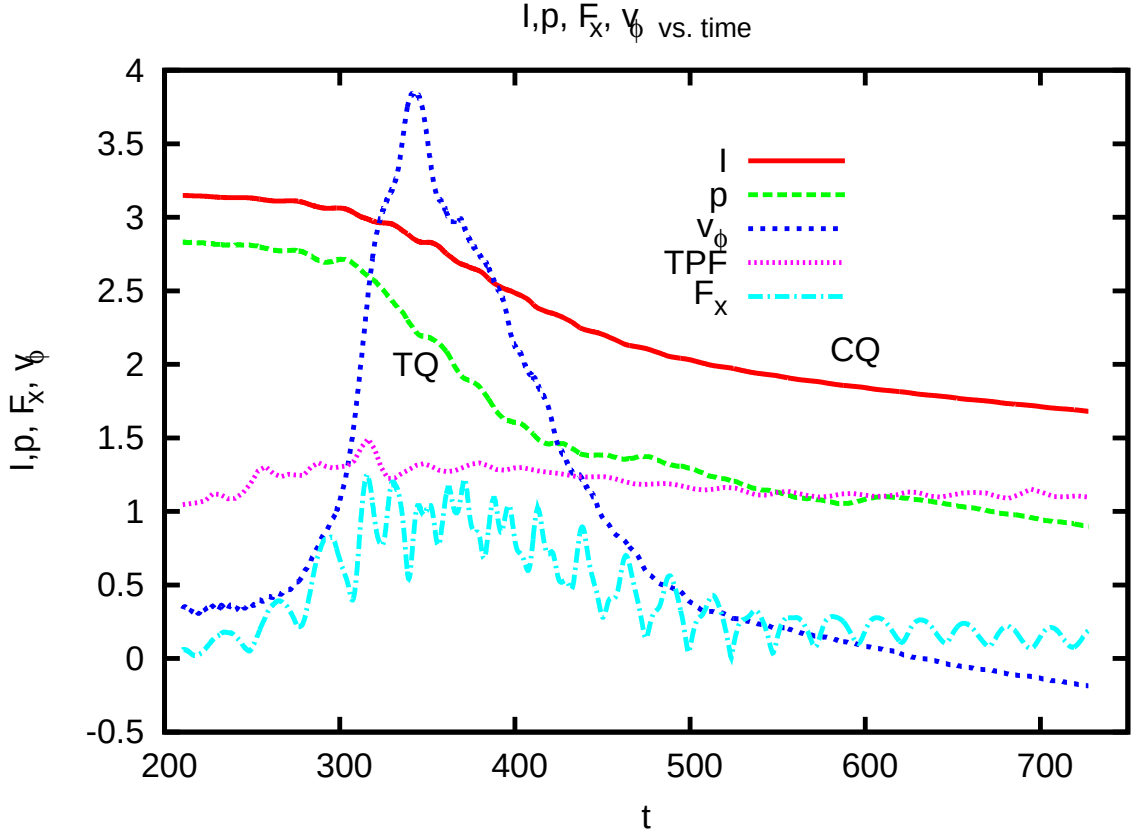

Time history of the simulation shown in previous figures. Shown are normalized total current I, total pressure P, V_ϕ, and F_x. $V_\phi = L_\phi / \int \rho R^2 dR dZ d\phi$, multiplied by 1000, so that $V_\phi \approx 0.004 v_A$. F_x, the sideways wall force, is multiplied by 10^4. The maximum $F_x \approx 3\%$ of the maximum force tolerable by ITER. The peak rotation coincides with the peak F_x. The rotation is counter - current: $V_\phi I_\phi / B < 0$.

Time history of sideways force

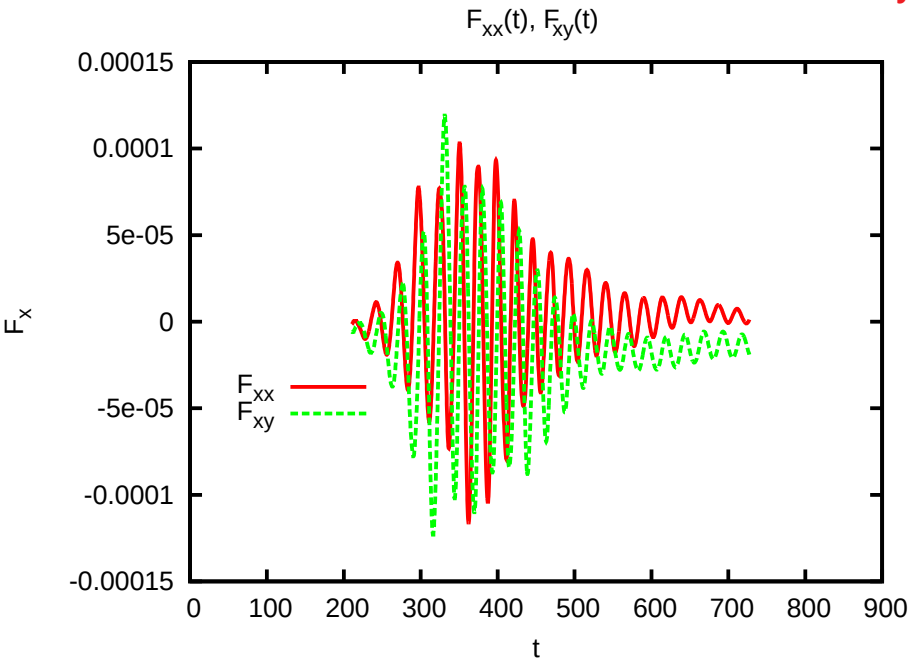

(a)

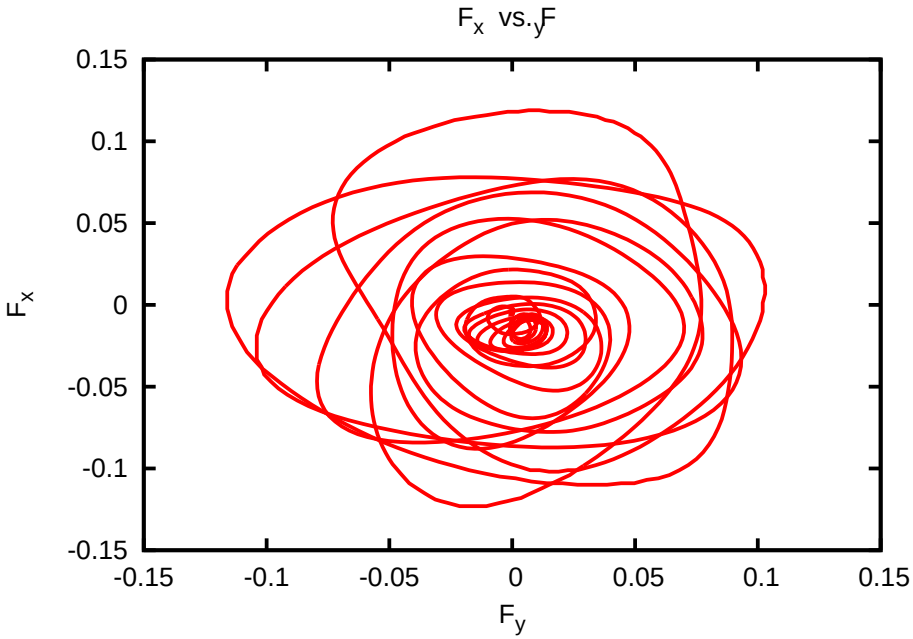

(b)

(a) Time history F_x, and the projections of the force in the $\hat{\mathbf{x}}$ and $\hat{\mathbf{y}}$ directions, $F_x = \mathbf{F} \cdot \hat{\mathbf{x}}$, and $F_y = \mathbf{F} \cdot \hat{\mathbf{y}}$. It can be seen that the direction of sideways force is rotating, with period comparable to the time the force is large. (b) same data, with $F_{xy}(F_{xx})$.

Time history of disruption 2

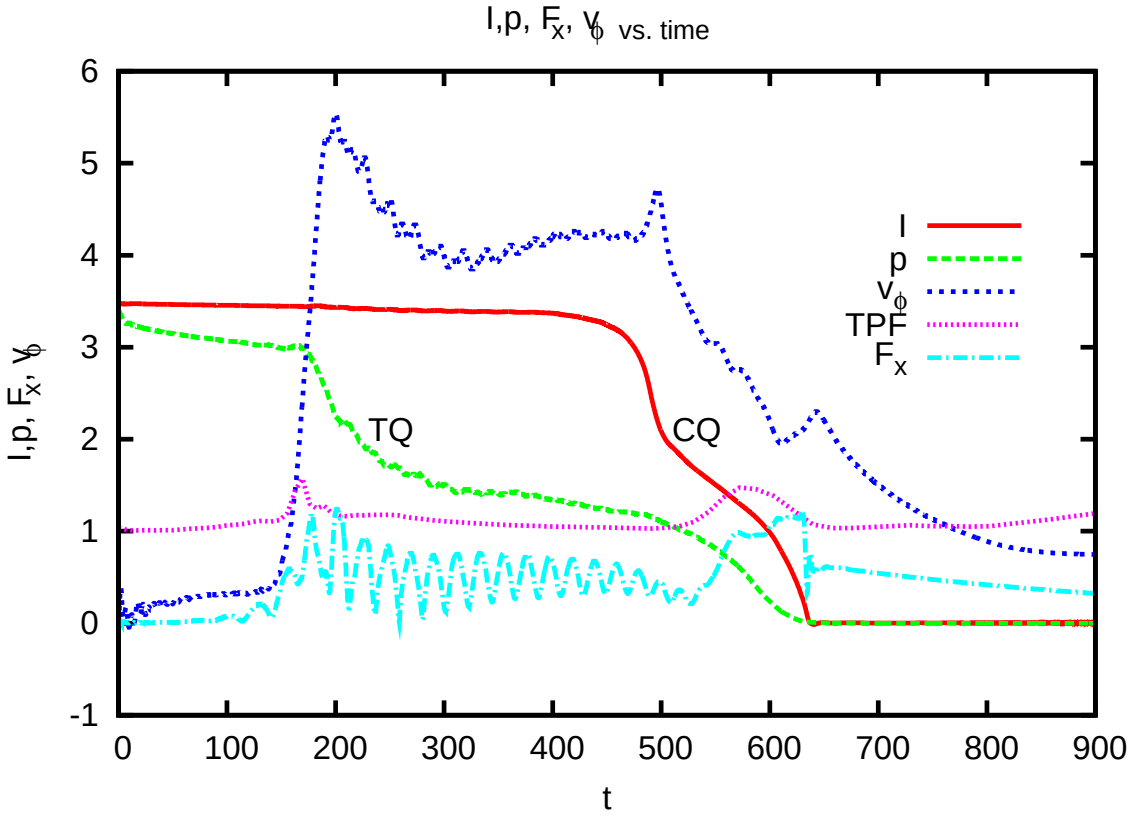

Time history of a simulation similar to the previous figures. In this case an external circuit model of the toroidal electric field sustains the current for $t \leq \tau_{CQ}$. The toroidal rotation is also sustained.

Numerical accuracy of toroidal angular momentum conservation

The dominant part of the toroidal force balance is

$$\int \rho R^2 \frac{\partial v_\phi}{\partial t} dV = \int \nabla G \times \nabla \psi \cdot \hat{\phi} dV + \ldots \tag{7}$$

The numerical implementation of (3) is in conservation form, because

$$\int_\Omega \nabla G \times \nabla \psi \cdot \hat{\phi} dR dZ = \oint_{\partial\Omega} G d\psi \tag{8}$$

for each element Ω.

Boundary Conditions allow $\dot{L}_\phi \neq 0$

ψ and G satisfy resistive wall boundary conditions

$$\frac{\partial \psi}{\partial t} = \frac{\eta_{wall}}{\delta}(\psi'_{vacuum} - \psi'_{plasma}) \tag{9}$$

$$\eta G' = \frac{\eta_{wall}}{\delta}(G_{vacuum} - G_{plasma}) \tag{10}$$

ψ has Dirichlet boundary condition, but G has Neumann which permits $\partial G/\partial t \neq 0$ on the boundary.

Analytic model of rotation source

To express $\dot{L}_\phi$ in terms of magnetic perturbations, the magnetic fluxes ψ and G can be split into equilibrium and toroidally varying parts, $\psi = \psi_0 + \psi_1$, $G = G_0 + G_1 + G_2$. For simplicity we assume circular equilibrium cross sections, $dl = r d\theta$. The perturbed magnetic fluxes ψ, G approximately satisfy [Strauss 1977],

$$\psi_1 = \mathbf{B}_0 \cdot \nabla \xi \tag{11}$$

$$G_1 = -\nabla G_0 \times \nabla \xi \cdot \widehat{\phi} \tag{12}$$

$$G_2 = -\nabla G_1 \times \nabla \xi \cdot \widehat{\phi} \tag{13}$$

where ξ is the perturbation displacement potential, given by

$$\int^t \mathbf{v} dt' = \nabla \xi \times \widehat{\phi} \tag{14}$$

Then $G_1 = -(G_0'/r)\partial\xi/\partial\theta$. The change of G in next order is

$$G_2 \approx \frac{G_0'}{r^2} \frac{\partial}{\partial r} \left(\frac{\partial \xi}{\partial \theta} \right)^2 \tag{15}$$

The plasma is displaced by a VDE with $(m,n)=(1,0)$, $\psi_0=\psi_0(r-\xi_{10}\sin\theta)\approx -\xi_{10}\sin\theta\psi_0'$, $\xi=\xi(r-\xi_{10}\sin\theta,\theta,\phi)\approx -\xi_{10}\sin\theta\xi'$. This gives the result , with $\psi_1\approx 0$,

$$\dot{L}_\phi\approx\oint\frac{\partial\psi_0}{\partial\theta}G_2 d\theta d\phi\approx\frac{G_0'B\xi_{10}^3}{2qrR}\frac{\partial}{\partial r}\oint\left(\frac{\partial\sin\theta\xi'}{\partial\theta}\right)^2\cos\theta d\theta d\phi. \tag{16}$$

We must have at least two modes $(m,n),(m+1,n)$ contributing to ξ, which beat together to give a $\cos\theta$ term. It is useful to express (16) using (5) in terms of B_θ,

$$\xi=\sum_m\xi_{mn}\sin(m\theta-n\phi),\qquad B_\theta=\sum_{mn}B_{\theta mn}\cos(m-nq) \tag{17}$$

with

$$B_{\theta mn}\approx-\frac{B}{R}(\frac{m}{q}-n)\xi_{mn}' \tag{18}$$

which gives

$$\frac{dL_\phi}{dt}=\frac{\pi^2}{2}rqG_0'\xi_{10}^3\frac{R}{B}\sum_{mn}\frac{\partial}{\partial r}\left[\frac{m(m+1)B_{\theta mn}B_{\theta(m+1)n}}{(m-nq)(m+1-nq)}\right] \tag{19}$$

Rotation of F_x

We noted that F_x depends on the displacements ξ_{11}, ξ_{21}:

$$F_x = c_{21}\frac{\xi_{VDE}}{b}\frac{\xi_{21}}{a} + c_{11}\frac{\xi_{11}}{a}$$

where c_{11}, c_{21} depend on geometry, q, and $\gamma\tau_{wall}$. The displacements rotate with the plasma toroidal velocity:

$$\xi_{11} = \xi_{11}(r, \theta, \phi - v_\phi(r)t/R)$$

$$\xi_{21} = \xi_{21}(r, \theta, \phi - v_\phi(r)t/R),$$

which causes F_x to rotate. Note that ξ_{11}, ξ_{21} are localized in the plasma, where $v_\phi(r)$ is larger than at the wall, and that ξ_{11}, ξ_{21} are localized at different radii, causing possible beating and rotation reversal.

Rotation in ELMs

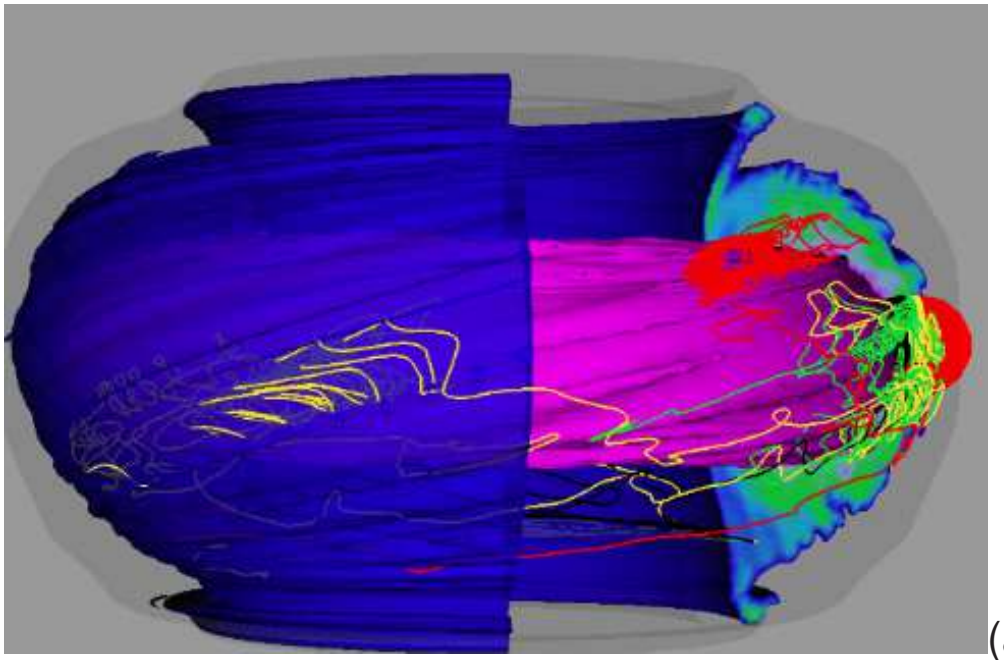

(a)

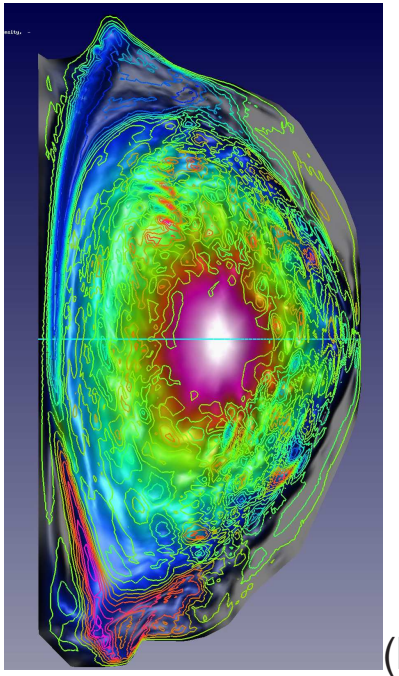

(b)

High resolution ELM simulation of DIII-D shot 126006. (a) two density isosurfaces, with velocity streamlines. Several of the streamlines follow the density corrugations, which in turn are parallel to the magnetic field. Near the edge the streamlines follow the ELM fingers. (b) contour plot of v_ϕ, has an approximately zonal structure, with different direction in the center and the edge. There is also a region of reversed v_ϕ at the separatrix in the bottom of the figure.

ELM simulation

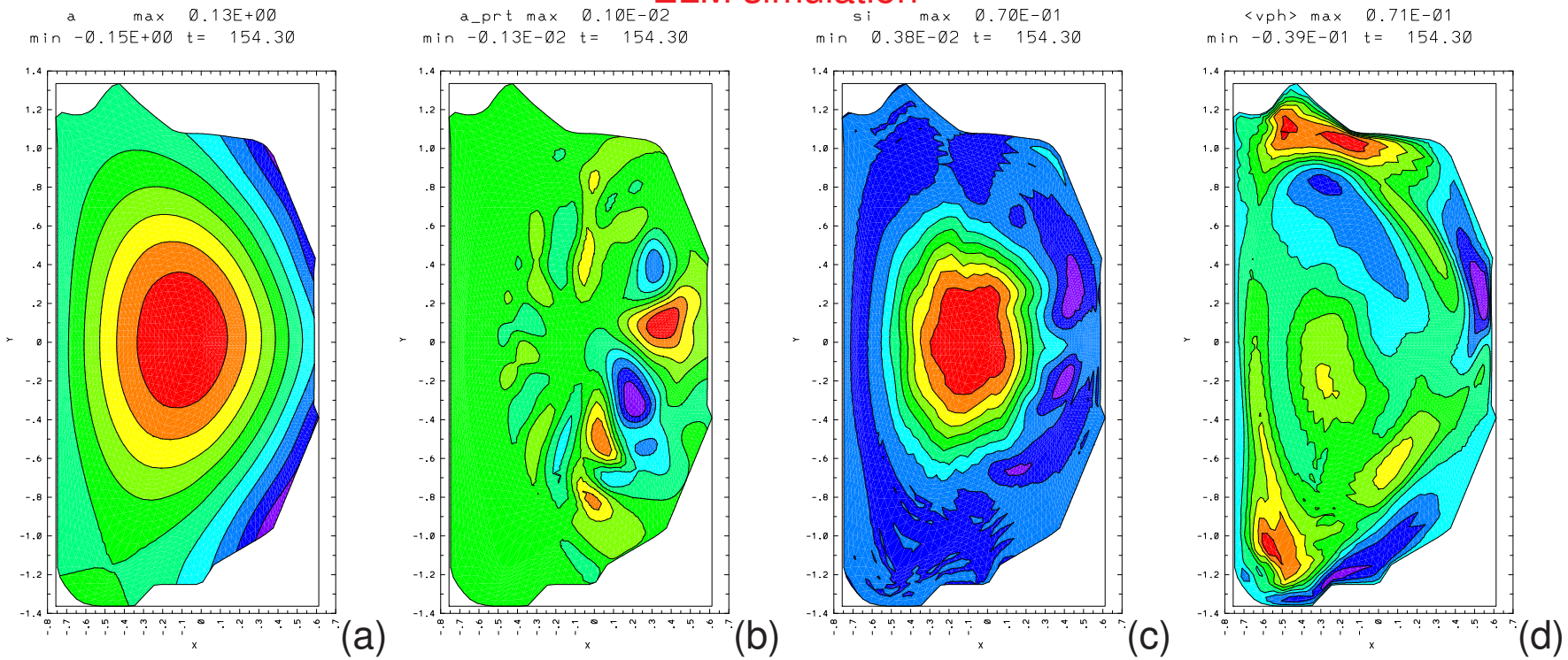

ELM simulation of DIII-D 126006, $S = 10^5, \tau_{wall} = 100\tau_A$. (a) The poloidal magnetic flux ψ at toroidal angle $\phi = 0$, time $t = 154\tau_A$. (b) perturbation of ψ. (c) toroidal magnetic flux G (d) Toroidally averaged toroidal velocity.

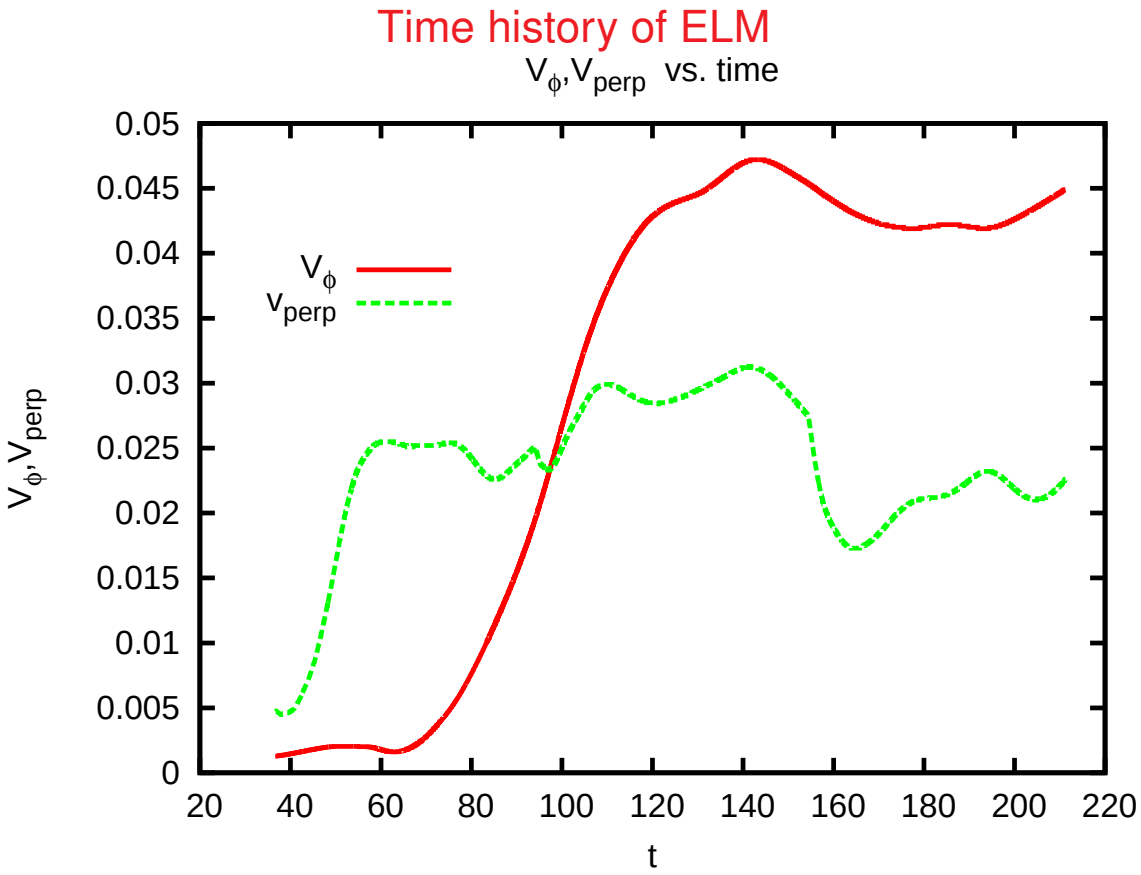

Time history of the simulation shown in previous figure. Shown are V_ϕ and $V_\perp$. The maximum value of $V_\phi = 0.05 v_A$. The results are insensitive to τ_{wall}/τ_A.

Intrinsic toroidal rotation

Scaling law of rotational Alfvén Mach number $M_\phi \propto \beta_N$ has been obtained where $M_\phi = v_\phi/v_A$. " ... scalings of intrinsic rotation with normalized gyro - radius or collisionality show no correlation. Whether this suggests the predominant role of MHD phenomena such as ballooning transport over turbulent processes in driving the rotation remains an open question." [Rice 2007] This was a comparative study of intrinsic toroidal rotation in H mode plasmas, in several experiments.

In a high β large aspect ratio approximation [Strauss 1977], $G_0 = -Rp/B$, so a β scaling emerges naturally. This tends to be a better approximation in an H mode pedestal, where there is a relatively large pressure gradient. The VDE could be replaced by vertical asymmetry, and the 3D perturbations could be ballooning modes which occur in ELMs. Writing (19) in terms of the normalized time $1/(\gamma\tau_A)$, and dividing both sides by $\rho\gamma\tau_A$ gives the scaling

$$M_\phi \approx \frac{\pi}{2\gamma\tau_A}\frac{\xi_{10}^3}{r^2R}\frac{m^2B_{\theta mn}^2}{B^2}\beta_N, \tag{20}$$

where $\beta_N = \epsilon pR/(BI_\phi)$.

Taking $\gamma\tau_A = 0.01$ as above, $B_\theta/B = 0.01$, $\xi_{10}/r = 0.5$, $m = 3$, and $\beta_N = 3$ yields

$$M_\phi \approx 1.6 \times 10^{-2} \tag{21}$$

consistent with the simulations above and with the ITER prediction of [Rice 2007].

Halo current

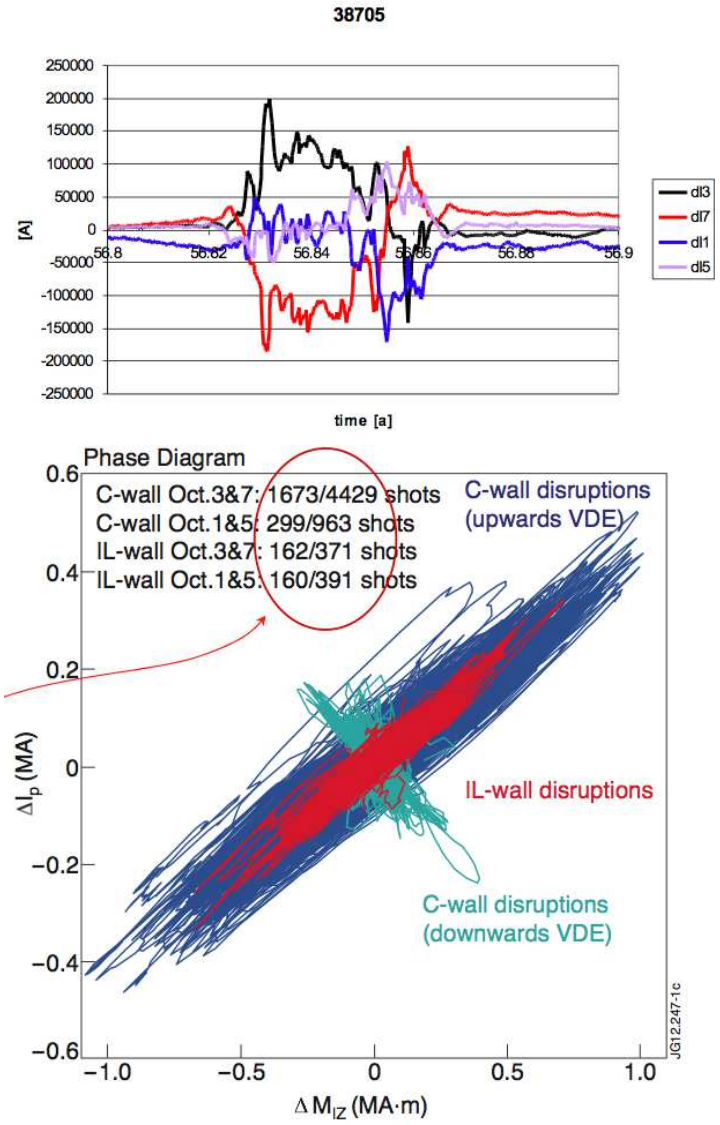

(a)

(b)

Toroidal variation of toroidal current

It was found in JET that during disruptions, the toroidal current varied with toroidal angle. It was found that $\Delta I_\phi / I_\phi \approx 0.08$, where ΔI_ϕ is the amplitude of the $n = 1$ variation.

(a) Current $I_\phi(\phi, t)$ measured in quadrants of JET, showing $n = 1$ toroidal variation.

(b) Toroidal current variation ΔI_ϕ vs. ΔM_{IZ}, vertical displacement of the current.

L. E. Zakharov, Phys. Plasmas **15** 062507 (2008).

S. N. Gerasimov *et al.,* Proc. of EPS 37th Conference on Plasma Physics (2010); S. N. Gerasimov ITPA meeting, Abingdon (2013).

These results can be explained in terms of 3D halo current.

Three dimensional halo current

The standard two dimensional halo current is

$$I_{halo} = \frac{1}{2}\oint |J_n| R dl \tag{22}$$

The three dimensional halo current is defined by

$$I_{halo3D} = \oint J_n R dl. \tag{23}$$

where the integral is along the plasma facing surface of the wall. Using $\nabla \cdot J = 0$, and integrating over a poloidal cross section, yields the

$$\frac{dI_\phi}{d\phi} = -I_{halo3D}. \tag{24}$$

We showed previously [Strauss *et al.* 2010] that

$$\Delta I_\phi = \frac{\xi_{vde}}{a^2}\Delta M_{IZ} \tag{25}$$

where $M_{IZ} = \int Z J_\phi dR dZ$, as in the previous figure, and

$$\Delta M_{IZ} = I_\phi \frac{a^2}{b}\frac{(2+\gamma_{11}\tau_{wall})(1-q_a)}{2b/a+\gamma_{11}\tau_{wall}(b/a-a/b)}\frac{\xi_{11}}{a} \tag{26}$$

From (25), the slope of the curves in the previous figure is positive (negative) for an upward (downward) VDE.

Halo current fraction

The halo current fraction is the ratio of halo current to toroidal plasma current, defined as

$$\mathrm{HF} = \frac{2\pi < I_{halo} >}{< I_{\phi} >}. \tag{27}$$

where the bracket denotes an average over the toroidal angle. The factor 2π appears in (27) because the total halo current $\int I_{halo} d\phi$ is needed, not the toroidal average.

The magnitude of the variation of the toroidal current can be expressed

$$\frac{\Delta I_{\phi}}{I_{\phi}} = \frac{I_{halo3D-max}}{< I_{\phi} >} = \frac{1}{2\pi} C_{halo} \times TPF \times HF \tag{28}$$

where

$$C_{halo} = \frac{I_{halo3D-max}}{I_{halo-max}} \tag{29}$$

and the toroidal peaking factor is

$$TPF = \frac{I_{halo-max}}{< I_{halo} >}. \tag{30}$$

A time history plot which continued from the VDE equilibrium shown previously with 3D perturbations, $S = 10^6, \tau_{wall} = 10^4 \tau_A$, shows

$$\mathrm{TPF}_{3D} = 1 + C_{halo}\mathrm{TPF}. \qquad (31)$$

which gives $C_{halo} \leq 0.5$, when $\mathrm{TPF}_{3D} \approx 1.6$ is a maximum, and $\mathrm{TPF} \approx 1.2$. Also plotted is $45\Delta I_\phi/I_\phi + 1$, well correlated with TPF_{3D}, which implies $\Delta I_\phi/I_\phi \approx 0.02$. This agrees with (28), taking $C_{halo} = 0.5, \mathrm{TPF} = 1.2, \mathrm{HF} = 0.2$.

Assuming $\gamma_{11}\tau_{wall} \gg 1$, we find [Strauss *et al.* 2013] $C_{halo} \leq \pi/2$, which gives

$$\frac{\Delta I_\phi}{I_\phi} \leq \frac{1}{4} \times TPF \times HF \leq \frac{3}{16} \qquad (32)$$

where $TPF \times HF \leq 0.75$, from experimental data.

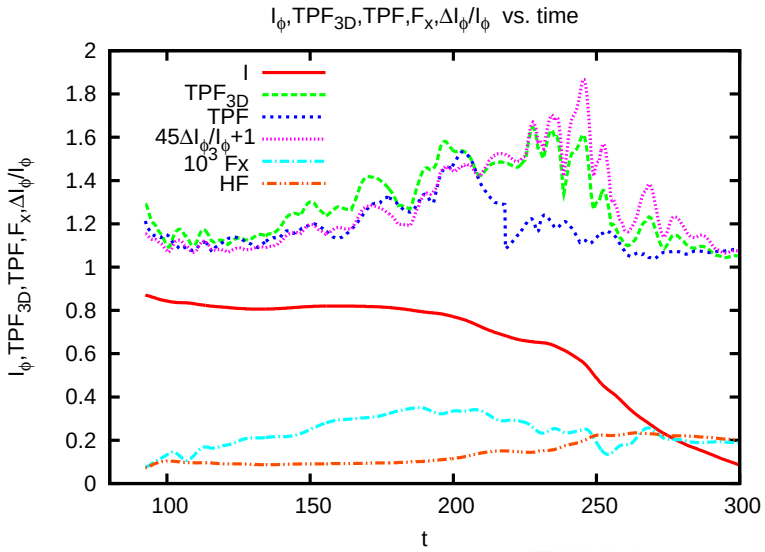

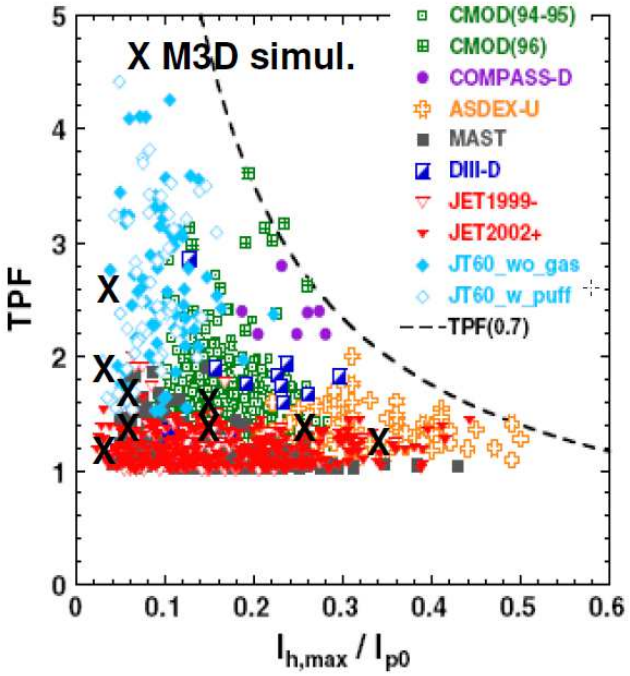

velocity boundary conditions

- Dirichlet: $v_n = 0$ – rigid wall
- Neumann: $\partial v_n/\partial n = 0$ – absorbing wall
- Robbins $\partial v_n/\partial n + \alpha v_n = 0$ – compromise

(a) $F_x(\gamma_{wall})$ for Neumann and Dirichlet velocity boundary conditions.

(b) $F_x(\alpha)$ with $\tau_{wall} = 20\tau_A$. Neumann for $\alpha = 0$, Dirichlet for $\alpha \to \infty$.

F_x(Neumann) $\approx 2 - 3 \times F_x$ (Dirichlet) for $\gamma\tau_{wall} \gg 1$.

Plasma is absorbed in about 10nm, much less than the resolution of MHD codes. Robbins with $\alpha \gg 1$ models short wall penetration depth and is approximately Dirichlet.

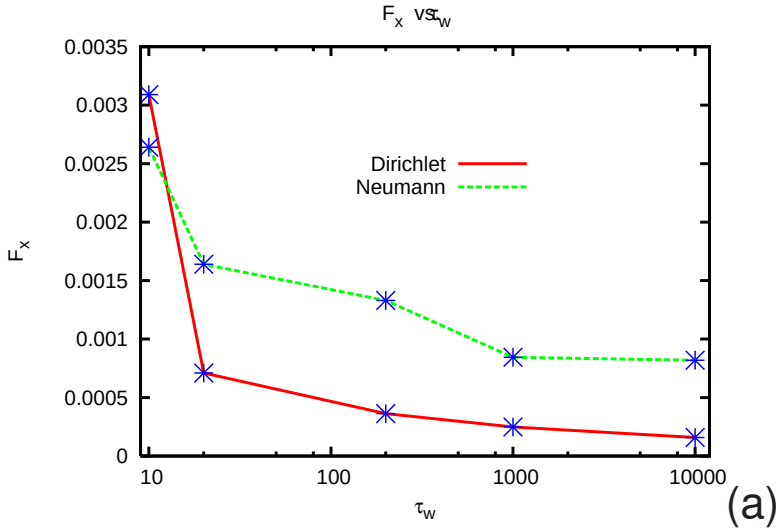

(a)

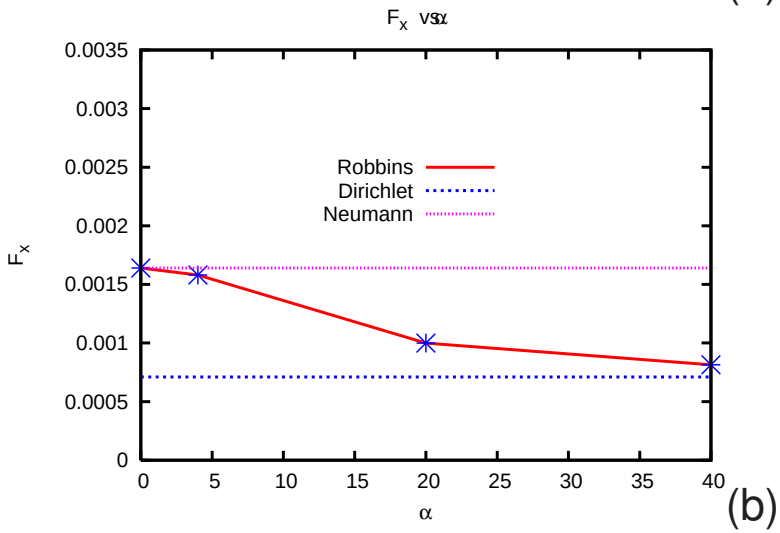

(b)

$v_\perp$ vs. $v_\parallel$ boundary conditions

The velocity is approximately

$$\mathbf{v} \approx \frac{\nabla\Phi \times \mathbf{B}}{B^2} + v_\parallel \frac{\mathbf{B}}{B} \tag{33}$$

Dirichlet: $\Phi = 0$ at boundary

Neumann: $\partial\Phi/\partial n = 0$ at boundary

On the outside of the wall, no vacuum electric field: $\Phi = 0$,

On the plasma side of the wall, must have $\Phi \approx 0$, or there will be very large electric field in the wall (in the 10 nm penetrated by plasma):

$E_{wall}/E_{plasma} \approx (\Delta\Phi_{wall}/10\text{nm})/(\Delta\Phi_{\text{plasma}}/1\text{m}) = 10^8$, if $\Delta\Phi_{wall} \sim \Delta\Phi_{plasma}$.

The parallel velocity $v_\parallel$ is not constrained: it can cause plasma to penetrate the wall. But it does not affect the magnetic field, hence does not affect halo current or wall force. It is small compared to $v_\perp$,

$$v_\parallel/v_\perp \sim \beta^{1/2} \ll 1.$$

$v_\parallel \sim$ hydrodynamic flow in a pipe, $v_\perp \sim$ salt water.

Notes on other disruption simulation approaches

Other suggested computational approaches do not include TQ, CQ, toroidal flow.

- 3D equilbrium code
  - TQ can not occur
    - involves breakup of flux surfaces and loss of equilibrium
  - no v_ϕ generation in equilibrium
- ideal MHD free boundary code
  - Plasma resistivity (for reconnection) is needed for TQ
  - Halo resistivity is needed for CQ

Conclusions

- AVDE disruptions have large variation in asymmetric wall force is F_x.
  - Asymmetric wall force is F_x maximum for $\gamma\tau_{wall} \sim 1$.
  - F_x is smaller for $\gamma\tau_{halo} \gg 1$, a mitigating effect
  - MGI mitigation of F_x depends offset linearly on VDE displacement.
- M3D simulation model can give TQ, CQ.
- Disruptions and ELMs can drive toroidal and poloidal rotation.
  - Toroidal rotation is sheared, MHD zonal flow.
  - toroidal rotation sustained for $t \approx \tau_{CQ}$.
  - ELM activity may produce intrinsic toroidal rotation, with $M_A \sim 10^{-2}$.
- 3D halo current produces toroidal variation of toroidal current. Toroidal current variation is limited to $3/16$ of the total toroidal current.
- $v_n = 0$ is a reasonable boundary condition.